Biosensors and Bioelectronics xxx (2016) xxx-xxx

Contents lists available at ScienceDirect

Biosensors and Bioelectronics

journal homepage: www.elsevier.com

Interactions between bacterial surface and nanoparticles govern the performance of "chemical nose" biosensors

Mohit S. Verma,[a, b] Shih-Chung Wei,[d] Jacob L. Rogowski,[a, b] Jackson M. Tsuji,[a] Paul Z. Chen,[a, b] Chii-Wann Lin,[d, e] Lyndon Jones,[a, c] Frank X. Gu[a, b, *]

[a] Department of Chemical Engineering, University of Waterloo, 200 University Avenue W, Waterloo, Ontario N2L 3G1, Canada
[b] Waterloo Institute for Nanotechnology, University of Waterloo, 200 University Avenue W, Waterloo, Ontario N2L 3G1, Canada
[c] Centre for Contact Lens Research, University of Waterloo, 200 University Avenue W, Waterloo, Ontario N2L 3G1, Canada
[d] Institute of Biomedical Electronics and Bioinformatics, National Taiwan University, No. 1, Section 4, Roosevelt Road, Taipei 10617, Taiwan
[e] Institute of Biomedical Engineering, National Taiwan University, No. 1, Section 4, Roosevelt Road, Taipei 10617, Taiwan

ARTICLE INFO

Article history:
Received 22 February 2016
Received in revised form 6 April 2016
Accepted 8 April 2016
Available online xxx

Keywords:
Colorimetric
Lipid blots
Extracellular polymeric substances
Pathogens
Modeling
Gold nanoparticles

ABSTRACT

Rapid and portable diagnosis of pathogenic bacteria can save lives lost from infectious diseases. Biosensors based on a "chemical nose" approach are attracting interest because they are versatile but the governing interactions between bacteria and the biosensors are poorly understood. Here, we use a "chemical nose" biosensor based on gold nanoparticles to explore the role of extracellular polymeric substances in bacteria-nanoparticle interactions. We employ simulations using Maxwell-Garnett theory to show how the type and extent of aggregation of nanoparticles influence their colorimetric response to bacteria. Using eight different species of Gram-positive and Gram-negative bacteria, we demonstrate that this "chemical nose" can detect and identify bacteria over two orders of magnitude of concentration (89% accuracy). Additionally, the "chemical nose" differentiates between binary and tertiary mixtures of the three most common hospital-isolated pathogens: *Staphylococcus aureus*, *Escherichia coli*, and *Pseudomonas aeruginosa* (100% accuracy). We demonstrate that the complex interactions between nanoparticles and bacterial surface determine the colorimetric response of gold nanoparticles and thus, govern the performance of "chemical nose" biosensors.

1. Introduction

Conventional biosensors focus on a 'lock and key' recognition strategy (Rotello, 2009), which utilizes biomolecules such as aptamers and antibodies to offer high sensitivity and specificity. (Verma et al., 2015b; Chung et al., 2013; Jung et al., 2010; Torres-Chavolla and Alocilja, 2009; Lazcka et al., 2007) However, developing broad-spectrum biosensors using this strategy is cumbersome because each target requires the use of a unique biomolecule. An alternative method for developing versatile biosensors involves the use of a "chemical nose" where a set of interactions between the pathogen and sensors produces unique patterns of response, in a manner similar to the functioning of our sense of smell (Bunz and Rotello, 2010; Miranda et al., 2010; Rotello, 2009). Designing a "chemical nose" biosensor requires minimal prior knowledge of the analyte because the system can be 'trained' to recognize various analytes (Rotello, 2009). Such "chemical nose" sensors have been used for detecting various targets such as amino acids (Folmer-Andersen et al., 2006), proteins (De et al., 2009), carbohydrates (Wright et al., 2005), volatile organic compounds (Peng et al., 2009), bacteria (Li et al., 2014; Verma et al., 2014b; Wan et al., 2014; Phillips et al., 2008), and cancer cells (Rana et al., 2015; Bajaj et al., 2010; Bajaj et al., 2009; El-Boubbou et al., 2007).

Typically, nanoparticle-based "chemical nose" biosensors require the modification of nanoparticle surface with multiple ligands where each ligand is responsible for a unique interaction with the target (Wan et al., 2014; Bunz and Rotello, 2010). These interactions have only been studied in a limited manner (Abadeer et al., 2015; Yang et al., 2015; Hayden et al., 2012) and thus, their role in the performance of "chemical nose" biosensors is poorly understood. The use of multiple ligands limits the ability to study the nanoparticle-bacteria interactions because of increased complexity in synthesis. Here, we have utilized a single molecule, cetyltrimethylammonium bromide (CTAB)—a typical surfactant used for synthesis of gold nanoparticles—for providing electrostatic and hydrophobic interactions between nanoparticles with various morphologies and surface features of bacteria. CTAB-coated nanoparticles have previously been employed for detection of bacteria (Verma et al., 2014a, 2014b, 2015a), but the interactions between these nanoparticles and components of bacterial surface have not been studied.

Here, we demonstrate the crucial role of extracellular polymeric substances (EPS) in controlling the response of the "chemical nose" to the different bacterial species using lipid blot assays and transmission electron microscopy (TEM). Simulations of gold nanoparticle aggregation highlight that different types of aggregates are responsible for producing unique colorimetric responses to different species of bacteria. In the current study, we use this "chemical nose" to not only detect and identify eight different species of Gram-positive and Gram-negative bacteria at three different concentrations, but also discriminate between polymicrobial mixtures.

* Corresponding author at: Department of Chemical Engineering, University of Waterloo, 200 University Avenue W, Waterloo, Ontario N2L 3G1, Canada.
Email address: frank.gu@uwaterloo.ca (F.X. Gu)

http://dx.doi.org/10.1016/j.bios.2016.04.024
0956-5663/

2. Materials and methods

2.1. Materials

Gold (III) chloride hydrate (HAuCl4·xH2O), cetyltrimethylammonium bromide (CTAB), sodium borohydride, silver nitrate, hydrochloric acid, nitric acid, sodium hydroxide, L-ascorbic acid, Amersham™ Protran® Supported nitrocellulose (NC, 0.2 μm pore size) membrane, lipopolysaccharides (LPS-S) from *Pseudomonas aeruginosa* 10, rough strain (Rd) lipopolysaccharides (LPS-R) from *Escherichia coli* F583, peptidoglycan (PepG) from *Staphylococcus aureus*, and lipoteichoic acid (LTA) from *S. aureus* were purchased from Sigma-Aldrich (Oakville, ON, Canada). Trisodium citrate dihydrate was purchased from Thermo Fisher Scientific (Burlington, ON, Canada). Transparent, sterile 96-well microplates, scintillation vials (20 mL), BD trypticase soy agar (TSA) culture plates, BD TSA with 5% Sheep Blood (TSA II) culture plates, BD nutrient broth, sodium chloride (ACS grade), Nalgene sterilization filter units (0.2 μm pore size), calcium alginate swabs, and Amersham™ Hybond™ polyvinylidene difluoride (PVDF, 0.45 μm pore size) membrane were purchase from VWR (Mississauga, ON, Canada). 400 mesh formvar/carbon coated copper grids were purchased from Canemco Inc (Gore, QC, Canada). Cardiolipin (CL), L-α-phosphatidylglycerol (PG), and L-α-phosphatidylethanolamine (PE) from *E. coli* were purchased from Avanti Polar Lipids (Alabaster, AL, USA). *P. aeruginosa* (ATCC 9027), *S. aureus* (ATCC 6538), *E. coli* (ATCC 10798), *Achromobacter xylosoxidans* (ATCC 27061), *Delftia acidovorans* (ATCC 15668), *Stenotrophomonas maltophilia* (ATCC 13637), *Enterococcus faecalis* (ATCC 29212) and *Streptococcus pneumoniae* (ATCC 6305) were purchased from Cedarlane Labs (Burlington, ON, Canada). All procured chemicals were used without further purification. The 20 mL vials used for gold nanoseed synthesis were cleaned using 12 M sodium hydroxide and larger glassware was cleaned using aqua regia as described in published protocol (Liu and Lu, 2006).

2.2. Synthesis of gold nanoparticles

The gold nanoseed precursor was synthesized using a previously described simple two-step one pot process (Verma et al., 2014a, 2014b; Lu et al., 2010). Briefly, 60 μL of 0.1 M freshly prepared ice-cold sodium borohydride was added to 20 mL of a gold (III) chloride hydrate (2.4×10^{-4} M) and trisodium citrate dihydrate (10^{-4} M) solution under vigorous stirring. The sample was incubated overnight in the dark in ambient conditions, filtered (0.2 μm) and stored at 4 °C until use. To synthesize branched gold nanoparticles, a previously published procedure employing CTAB as a negative template was used with changes in the amount of silver nitrate to get a greater distinction between the morphologies of nanoparticles (Verma et al., 2014a, 2014b). Briefly, 210 mL of 7.33 mM CTAB and 1.46 mM CTAB were used for branched and spherical nanoparticles respectively. Gold (III) chloride hydrate (8.97 mL, 11 mM) was added to each CTAB solution, followed by silver nitrate (1.34 mL for branched nanoparticles and 0.67 mL for spherical nanoparticles, 10 mM) under moderate stirring. Then, L-ascorbic acid (1.44 mL, 100 mM) was added dropwise and the solution turned clear. The appropriate volume of gold nanoseed (2.24 mL for branched nanoparticles and 5.60 mL for spherical nanoparticles) was immediately added. The nanoparticles were purified by centrifugation at 10,000 rpm for 15 min resuspended in 1 mM CTAB solution. These two gold nanoparticle solutions were mixed (1:1 by volume) to obtain the purple "chemical nose" solution.

2.3. Bacterial culture

P. aeruginosa, S. aureus, E. coli, A. xylosoxidans, D. acidovorans, and *S. maltophilia* were inoculated on Trypticase Soy Agar (TSA) plates and incubated at 37 °C for 24 h. *E. faecalis* and *S. pneumoniae* were inoculated on TSA II plates and incubated at 37 °C for 24 h, where *S. pneumoniae* was placed in a 5% CO_2 environment. Bacterial cells were harvested using alginate swabs and suspended in 5 mL of sterile saline (2.55%) with nutrient broth (~0.006%) in a 15 mL centrifuge tube. In the case of *S. pneumoniae,* cultures from two TSA II plates were combined due to low OD_{660} values of the culture, which is used for normalization. Each bacterial strain was then washed seven times with 2.55% saline (with ~0.006% nutrient broth) by centrifugation at 4000 rpm for 10 min. The bacteria were then diluted to obtain an optical density at 660 nm (OD_{660}) of 0.10 ± 0.005 (~10^8 CFU/mL) (Dantam et al., 2011). The wavelength of 660 nm was chosen because it has previously been used for similar bacteria (Dantam et al., 2011). When the bacteria are added to gold nanoparticles, the solution is diluted 1:3 to obtain final OD_{660}=0.03 for bacteria. The actual concentrations of bacteria were determined by plate count method and are summarized in Table S1. Other concentrations of bacteria were obtained by diluting the solutions 1:5 or 1:25 in 2.55% saline (with ~0.006% nutrient broth). In order to study the concentration dependent response (Fig. S7), the bacterial solutions were normalized to an OD_{660} of 1.0 ± 0.05 and then diluted 1:16, 1:32, 1:64, 1:128, 1:256 and 1:512. In the current study, all bacteria were grown at the same time and the effect of different growth phases on the colorimetric response was not studied. It is expected that the growth phases might alter the cell surface and hence, this aspect will be explored in future studies.

2.4. Removal of extracellular polymeric substances (EPS)

An EPS extraction protocol was used on *S. aureus, E. coli,* and *A. xylosoxidans* with a slight modification of published method (Liu and Fang, 2002). The bacteria were first incubated on TSA plates at 37 °C for 24 h. Bacterial cells were harvested using alginate swabs and suspended in 10 mL of sterile saline (2.55%) with nutrient broth (~0.006%) in 15 mL centrifuge tubes. 60 μL of formaldehyde was added to a 5 mL aliquot of the bacterial suspension and the rest of suspension was used as a control. The tubes were incubated at 4 °C for 1 h. Then, 4 mL of 1 M sodium hydroxide was added to the treatment tube and saline was added to control tubes and incubated at 4 °C for an additional 3 h. In order to remove EPS from the cells, the bacteria were washed by centrifugation at 4000 rpm for 10 min seven times.

The bacteria concentration was then normalized to obtain $OD_{660} = 0.10\pm0.005$ (~10^8 CFU/mL) (Dantam et al., 2011) and 100 μL of bacteria were added to 200 μL of purple "chemical nose" solution in replicates of 4 in a microplate. The microplate was then placed on a Stovall Life Science Inc. (Peosta, IA, USA) Belly Dancer orbital shaker for 2 min and then incubated overnight under ambient conditions in the dark. Although the color change is visible within five minutes for some samples (Verma et al., 2014a), the color continues to evolve over time. The acquisition of absorption spectra for a microplate full of samples requires a few hours. Thus, the overnight incubation ensures that changes in spectra during acquisition are insignificant compared to the incubation time. After incubation, the UV–visible absorption spectra were obtained for each well in the microplates using a BioTek (Winooski, VT, USA) Epoch microplate spectrophotometer while scanning from 300 nm to 999 nm with a step size of 1 nm.

When extracting EPS for lipid blots, only *E. coli* was cultured on TSA plates and extracted using alginate swabs. First 60 µL of formaldehyde was added to 10 mL suspension of *E. coli* in saline and then treatment with sodium hydroxide was implemented as outlined above. The tubes were then centrifuged at 10,000 rpm for 30 min. Supernatant containing EPS was collected, filtered (0.2 µm), and dialysed (3500 Da) for 24 h at 4 °C before vacuum drying for 48 h.

2.5. Cell surface component blotting on membranes

Phospholipids (PG, PE, CL) were dissolved in chloroform to a final concentration of 2 mM. Other cell surface components (LPS-S, LPS-R, LTA, PepG) were dissolved or suspended in Millipore water to a final concentration of 2.86 mg/mL. Chloroform-based solutions were blotted onto PVDF in 2 µL volumes and water-based solutions were blotted onto NC in 2 µL volumes. Chloroform and water blanks (2 µL) were included on PVDF and NC blots, respectively. Membranes were then dried in the dark for 1 h under ambient conditions.

In order to test the effect of EPS, it was dissolved in Millipore water to a final concentration of 2.86 mg/mL (15×) and 0.191 mg/mL (1×). After drying, PG, PE, and CL blots on PVDF were overlaid with 30 µL of 1× EPS solution and vacuum dried for 2 h. Also, after drying of other component blots, 2 µL of 15× EPS solution was blotted overtop the LPS-S, LPS-R, LTA, and PepG blots and dried for an additional 1 h in the dark under ambient conditions. Control blots of chloroform- and water-based solutions were overlaid with 30 µL and 2 µL of Millipore water, respectively.

Once dried, membranes were transferred into a 10 mL bath of purple "chemical nose" solution and incubated on the Belly Dancer orbital shaker for 10 min. Following nanoparticle incubation, membranes were transferred to 100 mL of Millipore water and washed for 1 min with gentle shaking. Washed PVDF and NC membranes were photographed using a Canon EOS REBEL T3 digital camera. Image processing and data collection was done using ImageJ (National Institutes of Health). Images were first separated into RGB color channels. Background illumination was normalized by plotting Mean Green Values for 22–26 empty membrane regions (circular selection, 150 px diameter) against centroid coordinates. Linear regression was then performed using Microsoft Excel to generate x-and y-coordinate correction factors. Mean Green Values were then collected for each blot center (circular selection, 150 px diameter). These values were normalized for background illumination by applying the following transformation:

$$\mathrm{Value}_{\mathrm{corrected}} = \mathrm{Value}_{\mathrm{raw}} - x_{\mathrm{centroid}} * m_x - y_{\mathrm{centroid}} * m_y$$

where x and y are the x and y co-ordinates, m_x is the slope of the x co-ordinate vs. background green values, and m_y is the slope of the y co-ordinate vs. background green values.

Group means and standard deviations for each experimental condition were then determined using the corrected values and normalized against the control blots (chloroform+water and water+water, for PVDF and NC respectively). Statistical significance was determined in Microsoft Excel using one-tailed heteroscedastic *t*-tests.

2.6. Transmission electron microscopy

Red (spherical) and blue (branched) gold nanoparticle solutions were prepared for TEM by adding 5 µL to a copper grid and drying under ambient conditions overnight. Similarly, mixtures of bacteria and gold nanoparticles (5 µL) were added to formvar coated copper TEM grids and allowed to dry under ambient conditions overnight. Once dry, the bacterial samples were washed by placing 5 µL of Millipore water on the TEM grids for 30 s and then wicking the liquid using filter paper to remove excess surfactants, salts, and unbound gold nanoparticles. The samples were then imaged using a Phillips (Eindhoven, The Netherlands) CM10 TEM.

2.7. Modeling of gold nanoparticle aggregation

The optical characteristic of gold nanoparticle aggregates was estimated using Maxwell-Garnett effective medium theory (Ghosh and Pal, 2007). Here, spherical gold nanoparticles with a radius of 15 nm and six different types of aggregates (Fig. 5a) were simulated. Every aggregate was assumed to be a compact cluster which was smaller than optical wavelength and well-separated to other aggregates in solution. The effective permittivity (ε_{eff}) of these six different aggregation types was calculated with the Maxwell-Garnett equation:

$$\frac{\varepsilon_{\mathrm{eff}} - \varepsilon_s}{\varepsilon_{\mathrm{eff}} + 2\varepsilon_s} = V_a \times \frac{\varepsilon_a - \varepsilon_s}{\varepsilon_a + 2\varepsilon_s}$$

where V_a is the volume fraction of gold nanoparticles in solution as shown by boxes in Fig. 5a, ε_a is the complex permittivity of gold (Rakic et al., 1998), and ε_s is the permittivity of water (Wang and Lin, 2007). The absorption coefficient (α_{abs}) of the six aggregate types was then calculated (Bohren and Huffman, 2008):

$$\alpha_{\mathrm{abs}} = \frac{4\pi}{\lambda}\kappa = \frac{4\pi}{\lambda}\sqrt{\frac{\sqrt{\varepsilon_1^2 + \varepsilon_2^2} - \varepsilon_1}{2}}$$

where κ is the extinction coefficient, λ is the wavelength of light, and ε_1 and ε_2 denote the real and imaginary parts of effective permittivity of aggregates respectively.

The absorption spectrum of partially aggregated colloidal gold solutions was then predicted using a gold concentration of 0.10 mg/mL, which resembles the concentration of gold in the "chemical nose" after they are mixed with bacterial samples. First, the testing solution with one centimeter optical length was divided into many thin layers with a thickness of 120 nm each. The occupied volume and the composition of different aggregates were then assigned to each layer based on the information presented in Table 1. Then, the volume fraction and absorption coefficient of the free particles in the remaining volume were calculated. Finally, the absorption spectrum of the partially aggregated colloidal solution was determined using Beer-Lambert Law (Ricci et al., 1994; Swinehart, 1962):

Table 1.
Volume fractions occupied by the aggregate types shown in Fig. 5a and the percentage of total solution volume covered by the given aggregate type for various combinations

Aggregate type	Volume fraction (V_a)	Combination 1 (%)	Combination 2 (%)	Combination 3 (%)	Combination 4 (%)
Type 1	0.4189	0.0000000	0.0003000	0.0000000	0.0002000
Type 2	0.5236	0.0000000	0.0000020	0.0000000	0.0000200
Type 3	0.6046	0.0000080	0.0000400	0.0000400	0.0001000
Type 4	0.6910	0.0000070	0.0000140	0.0000175	0.0000700
Type 5	0.7255	0.0000050	0.0000200	0.0000300	0.0000500
Type 6	0.7441	0.0000065	0.0000260	0.0000390	0.0000650

$$A = -\log\left(\frac{I}{I_0}\right) = -\log(e^{-\alpha z}) = -\log(e^{-\alpha_1 z_1 - \alpha_2 z_2 - \alpha_3 z_3 \cdots})$$

where A is the absorbance, I_0 is the incident light intensity, I is the transmitted light intensity, α is the absorption coefficient, and z is the optical length. The optical length z for different types of aggregate was weighted by the percent volume occupied by aggregates (Table 1). It should be noted that Maxwell-Garnett effective medium theory is suitable for isolated particles where interaction between particles is ignored (Niklasson et al., 1981). The model assumes one material as the host and considers the volume fraction of the other material.

2.8. Identification and quantification of bacteria

The assay for identification and quantification of bacterial species was performed in 96-well microplates. The plates were prepared by adding 100 μL of the bacteria or saline control in replicates of eight. This was followed by the addition of 200 μL of the purple "chemical nose" solution and the microplates were incubated overnight before measuring the absorption spectra.

The training set was obtained by selecting three replicates out of eight and the other five replicates were randomized by an independent researcher. The researcher performing data analysis remained blind to the identity of the randomized samples. Using MathWorks® MATLAB®, hierarchical clustering analysis (HCA) based on Euclidean distance and Ward's method was performed on the training set of bacteria with OD_{660}=0.03. The corresponding dendrogram is presented in Fig. 7a. For classification, the training set was used to perform principal component analysis (PCA) and obtain the corresponding scores as well as coefficients. These principal component scores were used in the training of the linear discriminant analysis (LDA). Since obtaining the principal scores requires normalization by the mean of each response (wavelength), the randomized samples were normalized by these mean values and then translated to principal scores using the coefficients obtained from PCA. The gold nanoparticles show a unique spectral shift for each bacterial species and thus, the shape of the absorption spectra is unique for each species. Thus, all 700 wavelengths (300–999 nm) were used for PCA instead of selecting specific wavelengths to avoid biasing the data towards one specific pattern. Also, the use of all wavelengths allows this analysis to be adaptable if a more complex mixture of nanoparticles is used with multiple absorption peaks. PCA will assign a low weight to the wavelengths that do not significantly contribute to the variance of responses. The PCA scores were used in LDA to determine the group to which the unknown samples belonged, where each group corresponds to either saline control or a bacterium at a particular concentration. The principal component scores were plotted in Fig. S5 and the corresponding HCA dendrogram is plotted in Fig. S6.

Furthermore, a concentration dependent response for each bacterial species was obtained by normalizing each species to OD_{660} = 1.0±0.05, then diluting them in 2.55% saline 16×, 32×, 64×, 128×, 256×, and 512×. Then, 100 μL of each of these dilutions was added to 200 μL of the purple gold nanoparticle solutions and absorption spectra were obtained after overnight incubation. After obtaining the absorption spectra, the normalized absorbance values were calculated for all samples using the following equation:

$$\text{Normalized absorbance} = (\textit{Average saline control absorbance at } 540\ nm - \textit{Average saline control absorbance at } 800\ nm) - (\text{Sample absorbance at } 540\ nm - \text{Sample absorbance at } 800\ nm)$$

where absorption at 800 nm serves as a baseline. The normalized absorbance is plotted for each bacterial species in Fig. S7 assuming that OD_{660} = 1.0 has an approximate concentration of 10^9 CFU/mL (Dantam et al., 2011).

2.9. Identifying mixtures of bacteria

Mixtures of *P. aeruginosa, S. aureus* and *E. coli* were prepared by using the OD_{660} = 0.10±0.005 solutions and mixing them 1:1 and 1:1:1 by volume for binary and tertiary solutions respectively. Saline control and each of the bacteria samples were added to the 96-well microplate as before, and then the purple "chemical nose" solution was added and mixed. Three out of eight replicates were used as a training set, while the other five were randomized and used for identification. PCA and LDA were performed using MATLAB® as before.

3. Results and discussion

3.1. Role of EPS

We used a 1:1 volume mixture of CTAB-coated spherical and branched gold nanoparticles (Fig. S1) to obtain a purple colored solution as a "chemical nose." The difference in size and morphology of gold nanoparticles is chosen such that each set of particles can respond to the various species of bacteria in a unique manner and thus provide additional features to the absorption spectrum (Verma et al., 2014a, 2014b). When the solution of gold nanoparticles is added to bacteria, the nanoparticles aggregate around the bacteria due to electrostatic interactions between the cationic CTAB and anionic segments of cell walls. This aggregation leads to a color change due to a shift in the localized surface plasmon resonance. The color change is characterized by obtaining absorption spectra in the presence of various bacteria (Fig. 1). The aggregation around bacteria is mostly caused by teichoic acids in Gram-positive bacteria and lipopolysaccharides and phospholipids in Gram-negative bacteria (Verma et al., 2014b; Hayden et al., 2012; Sun et al., 2012; Phillips et al., 2008; Hong and Brown, 2006; Berry and Saraf, 2005; Berry et al., 2005).

EPS are present on the surface of bacteria and are expected to interact with nanoparticles and govern their aggregation. In order to confirm the effect of EPS, we executed an EPS extraction protocol for *S. aureus* (control)*, E. coli,* and *A. xylosoxidans* as per published methods (Liu and Fang, 2002). *S. aureus* serves as a control because it seems to lack EPS that would prevent binding of nanoparticles (Fig. 2, native). After extraction, the cells were mixed with the "chemical nose" solution and their colorimetric responses are presented in Fig. 1. A dramatic increase in response is observed for treated *E. coli* and *A. xylosoxidans* as compared native bacteria while the response of *S. aureus* does not change drastically. TEM images of the treated bacteria and gold nanoparticles (Fig. 2) are consistent with the colorimetric response where removal of EPS causes increased nanoparticle aggregation around *E. coli* and *A. xylosoxidans* while a similar coverage of nanoparticles is seen for treated and untreated *S. aureus.*

EPS can have an impact on various components of the cell surface such as phospholipids, lipopolysaccharides, teichoic acids, and peptidoglycan. EPS typically contain high fractions of carbohydrates and proteins (Liu and Fang, 2002), which could provide steric hindrance to the nanoparticles and thus cause a decrease in binding. In order to study the effects of EPS on these individual components, we used blot assays on PVDF and NC membranes to quantify nanoparticle binding. This strategy is adapted from protein lipid overlay assays for investigating the binding of proteins to lipids (Dowler et al., 2002). A

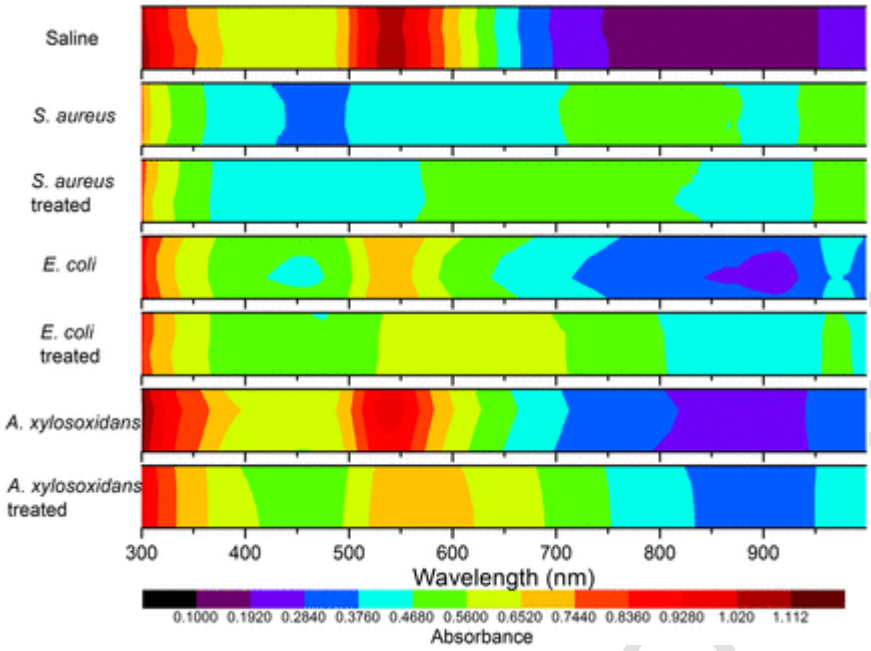

Fig. 1. Absorption spectra contour plots of gold nanoparticles in the presence of bacteria (n = 4) for each bacteria normalized to OD_{660}=0.03 and saline control, where each band consists of 4 slices (one per replicate). Each species was either tested in its native form or treated for removal of EPS using formaldehyde/sodium hydroxide method.

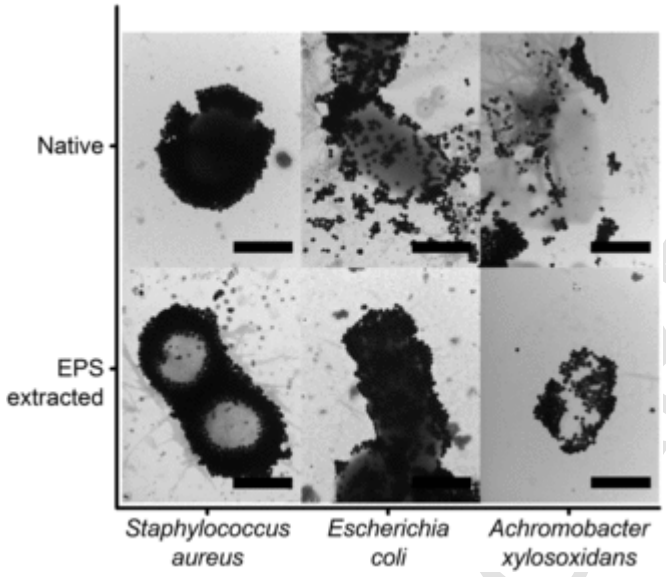

Fig. 2. TEM images of gold nanoparticles aggregating around bacteria with or without the extracellular polymeric substances (EPS) extracted. Scale bars are 500 nm each.

similar approach has been used for the detection of glycoproteins by immobilizing antibodies on the membrane and using peptide-coated gold nanoparticles (Zambre et al., 2012). PVDF was used for components that required chloroform for dissolution while NC was used for water-soluble components due to the hydrophobic and hydrophilic nature of PVDF and NC respectively. The visual binding of various cell surface components with and without EPS is presented in Fig. S2. Digital blot images can be characterized by analyzing color using RGB model (Vierck et al., 2000). Since the "chemical nose" absorbs mostly green light, we expect that an increased binding of nanoparticles to the membrane will show a decrease in the green component of RGB. The response is normalized by subtracting it from the background white color of the membrane. Fig. 3 highlights the binding of nanoparticles to various components of the cell walls. In the case of phospholipids, it is observed that at the same molar concentration, PG and diphosphatidylglycerol (cardiolipin, CL) demonstrate a higher binding compared to PE (Fig. 3a), which is expected because of the anionic nature of PG and CL and zwitterionic nature of PE. On the other hand, the water-soluble components have unknown molecular weights and hence cannot be directly compared to each other. All cell surface components demonstrate a significant reduction in binding of nanoparticles in the presence of EPS, except for LPS-R (Fig. 3a, b). Additionally, to confirm that the reduction in binding is due to the presence of EPS, various masses of EPS were added to PG blots by changing the concentration of EPS in solution. Fig. 3c highlights that increasing the mass of EPS leads to significant decrease in nanoparticle binding. Therefore, the presence of EPS is an important characteristic that determines the colorimetric response from the "chemical nose" biosensor.

3.2. Transmission electron microscopy analysis

In order to determine the response of these gold nanoparticles to other bacteria, a library of eight species (including both Gram-positive and Gram-negative) bacteria was mixed with the nanoparticles and their aggregation was observed by TEM. This aggregation of nanoparticles determines their colorimetric response when they are being used as a "chemical nose" biosensor. The TEM images presented in Fig. 4 highlight that in addition to *E. coli* and *A. xylosoxidans*, *D. acidovorans* also shows presentation of EPS, which prevents the aggregation of nanoparticles around the bacteria. In the case of *A. xylosoxidans* (Fig. 4d), gold nanoparticles aggregate between cells instead of on cells, which suggests that nanoparticles are not interacting strongly with the cellular surface. In other cases, the gold nanoparticles are heavily aggregated around the pathogen and adhere to the pathogen despite being rinsed once with water, which suggests strong electrostatic binding. Additionally, in cases of *P. aeruginosa* and *S. maltophilia,* the nanoparticles seem to aggregate around specific sections of the cell instead of evenly distributing throughout the surface

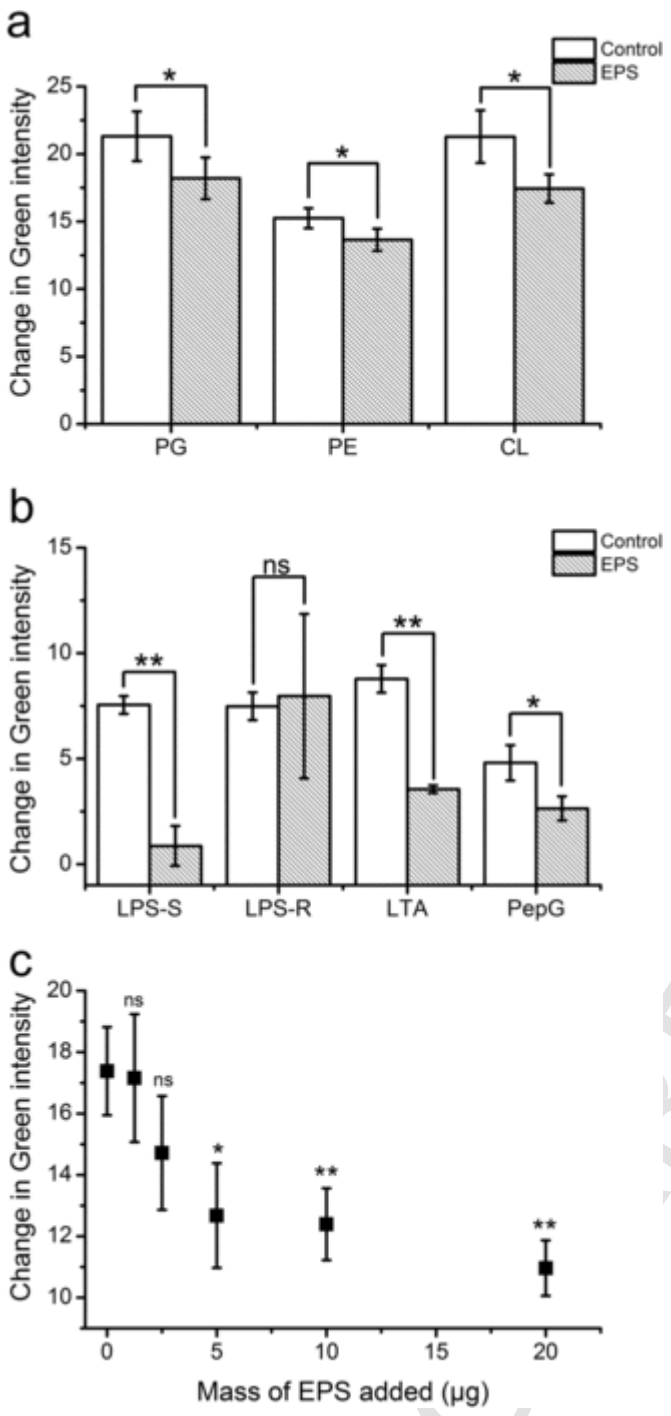

Fig. 3. Normalized Green intensity values from the RGB color model for images shown in Fig. S2: (a) Polyvinylidene difluoride (PVDF) membrane with L-α-phosphatidylglycerol (PG), L-α-phosphatidylethanolamine (PE), and cardiolipin (CL); (b) nitrocellulose membrane (NC) with smooth lipopolysaccharides (LPS-S), rough strain (Rd) lipopolysaccharides (LPS-R), lipoteichoic acids (LTA), and peptidoglyclan (PepG), and (c) PVDF membrane with PG and varying mass of extracellular polymeric substances (EPS). All values are reported as means±S.D. (n = 3), ns=not significant ($p \geq 0.05$),* $p \leq 0.05$, and ** $p \leq 0.01$.

(consistent with previous observation for *S. maltophilia* and branched gold nanoparticles (Verma et al., 2015b)), which could lead to a greater colorimetric response compared to other Gram-negative species. This also suggests the role of lipid domains that are present

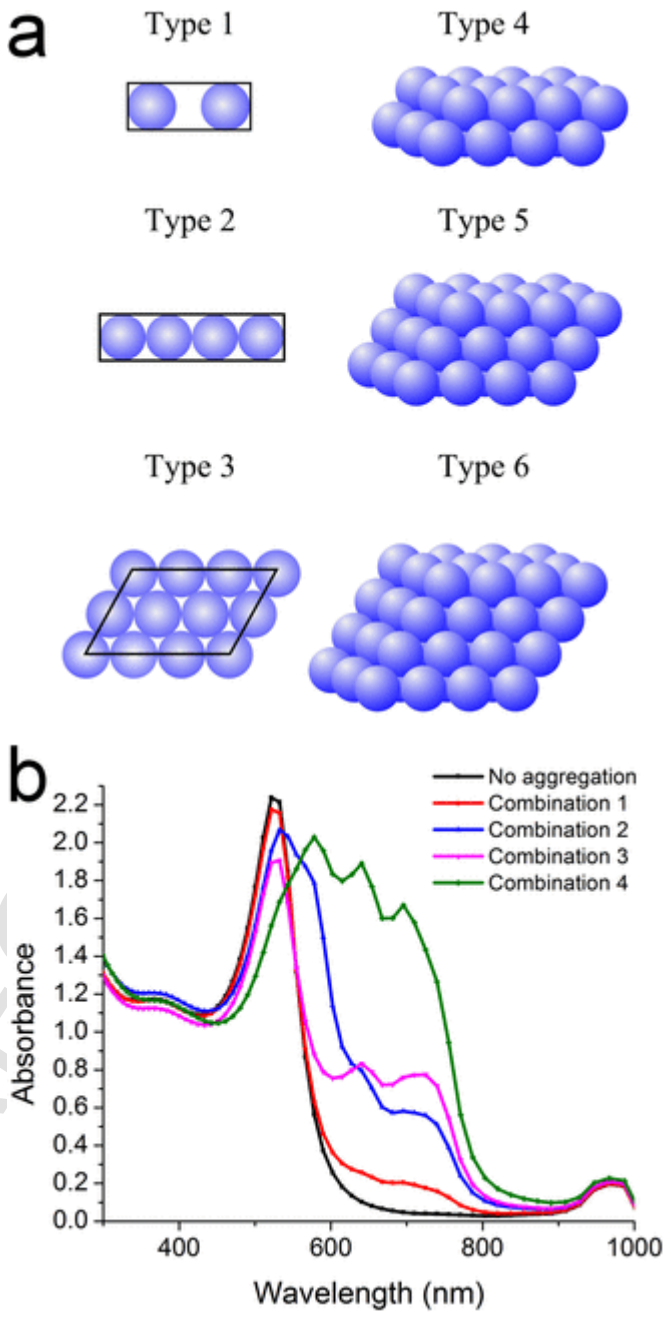

Fig. 4. TEM images of gold nanoparticles aggregating around bacteria: (a) *Pseudomonas aeruginosa*, (b) *Staphylococcus aureus*, (c) *Escherichia coli*, (d) *Achromobacter xylosoxidans*, (e) *Delftia acidovorans*, (f) *Stenotrophomonas maltophilia*, (g) *Enterococcus faecalis*, and (h) *Streptococcus pneumonia*.

around specific proteins (Matsumoto et al., 2006) or can form in the presence of cationic molecules such as CTAB (Epand and Epand, 2009). Specifically, PG and CL possess an overall negative charge which is expected to be probed by the cationic nanoparticles while PE being zwitterionic would show lower affinity as confirmed in the blot assays in Fig. 3a (Verma et al., 2014a). Yet, there are small differences between *P. aeruginosa* and *S. maltophilia* since more areas of *P. aeruginosa* seem to be bare (Fig. 4a) compared to *S. maltophilia* (Fig. 4f) and these differences can accumulate over the entire population of bacteria to magnify the aggregation state differences. Thus,

the nanoparticle aggregation is governed by the complex composition and configuration of the bacterial cell surface.

3.3. Modeling gold nanoparticle aggregation states

Different types of gold nanoparticle aggregates are observed in TEM images. Some bacteria lead to formation of multiple layers around the cell walls (Fig. 4b), while some have aggregates only in specific regions (Fig. 4a, f) and yet, some others have nanoparticles dispersed throughout the cell surface (Fig. 4c). In order to determine the relationship between gold nanoparticle aggregation type and their colorimetric response, we simulated aggregation of nanoparticles using Maxwell-Garnett effective medium theory (Ghosh and Pal, 2007), which has previously been implemented for metallic thin films (Donnelly et al., 2006; Ung et al., 2002; Dumont and Dugnoille, 1997) and particle clusters (Moskovits and Hulse, 1977). Six different types of gold nanoparticle aggregates were modeled, as shown in Fig. 5a and their ratios in solution were varied as described in Table 1. The expected absorption spectra in Fig. 5b show representative responses for different combinations of aggregate types. Each of these combinations shows a characteristic change for the response of gold nanoparticles to bacteria experimentally observed in Fig. 6a. The modeled spectra only consider spherical nanoparticles with fixed size and one type of aggregate packing (hexagonal close packed) while the "chemical nose" consists of a distribution of size and degree of branching of nanoparticles. Thus, the model provides coarse predictions compared to the experimental observations but the trends provide insight into the relationship between colorimetric response and aggregation on bacteria. Combination 1 uses a low total percent of aggregation using Type 3–6 aggregates. The obtained absorption spectrum correlates to the observed spectrum for *A. xylosoxidans* (Fig. 6a), which suggests that the overall degree of aggregation is low, as confirmed in TEM images (Fig. 4d). As we increase the overall percent of volume fraction occupied by aggregates in Combination 2 and introduce Type 1 aggregates, where nanoparticles are not in contact but rather separated by their radius, a slight peak shift is observed in addition to the increase in absorption in the 620 nm and 720 nm regions. The obtained absorption spectrum correlates to that of *D. acidovorans* (Fig. 6a), suggesting that some nanoparticles might be close to each other on the bacterial surface but not coming in contact. A further increase in planar and multi-layer stacking fraction in Combination 3 shows a significant drop of the 530 nm peak and an increase in the absorption at 620 nm and 720 nm, presenting a spectrum similar to the response from *E. coli* (Fig. 6a). Finally, Combination 4 has a significant fraction of nanoparticles aggregated including all types of aggregates and the absorption spectrum broadens significantly as is the case with *P. aeruginosa, S. aureus, E. faecalis, S. maltophilia,* and *S. pneumoniae.* These bacteria have a high fraction of aggregation either due to multiple layers around the cell wall (eg. *S. aureus* Fig. 4b) or due to patterns of aggregation (eg. *P. aeruginosa* Fig. 4a). In Combination 4, the absorbance at 530 nm also drops significantly due to the loss of free particles. Thus, Maxwell-Garnett effective medium theory provides some insight into how different types of nanoparticle aggregates around bacteria could be influencing the observed colorimetric changes and thus, how each bacterial species presents a distinguishable color change.

3.4. Identification and quantification of bacteria

The absorption spectra for gold nanoparticle-based "chemical nose" in the presence of bacteria are presented in Fig. 6a. These spectra demonstrate that the presence of bacteria causes broadening of the absorption peak due to higher absorption at longer wavelengths, which is typical for gold nanoparticle aggregation. Replicates for the

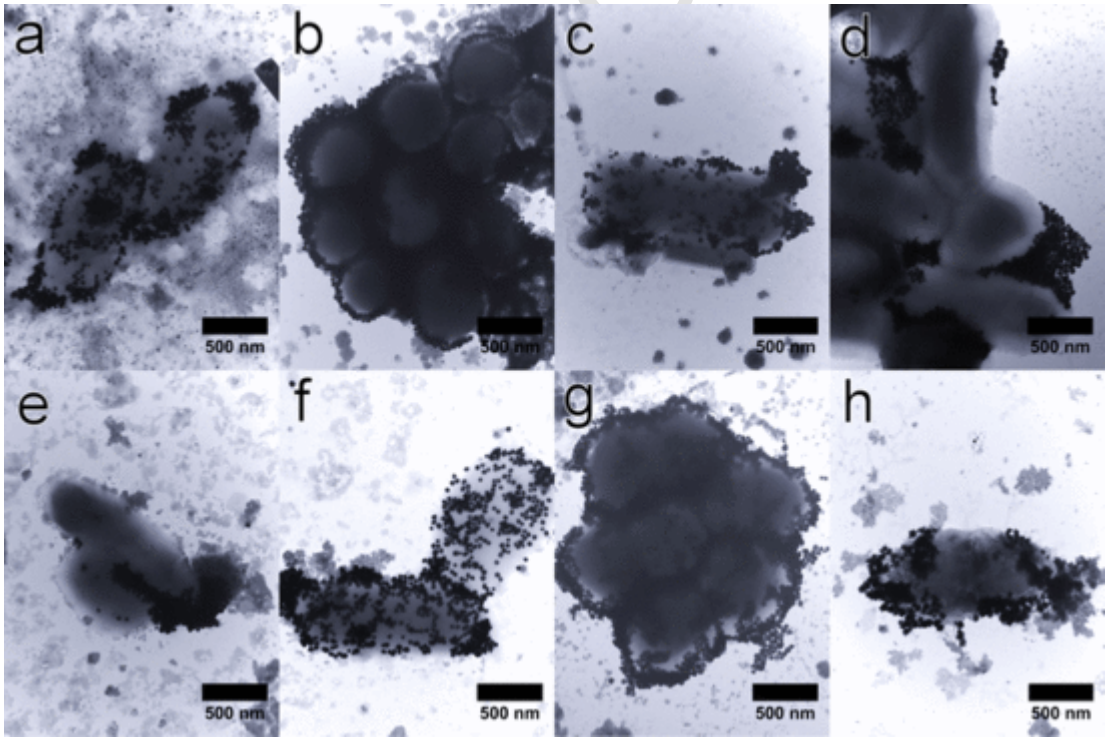

Fig. 5. Different types of nanoparticle aggregates and their modeled absorbance spectra: (a) schematic of aggregate types, the quadrilaterals in Types 1–3 indicates the volume used to calculate volume fraction occupied by the aggregate (V_a), a hexagonal close packed structure is used for Types 4–6; (b) absorbance spectra obtained for various combinations of aggregate types detailed in Table 1.

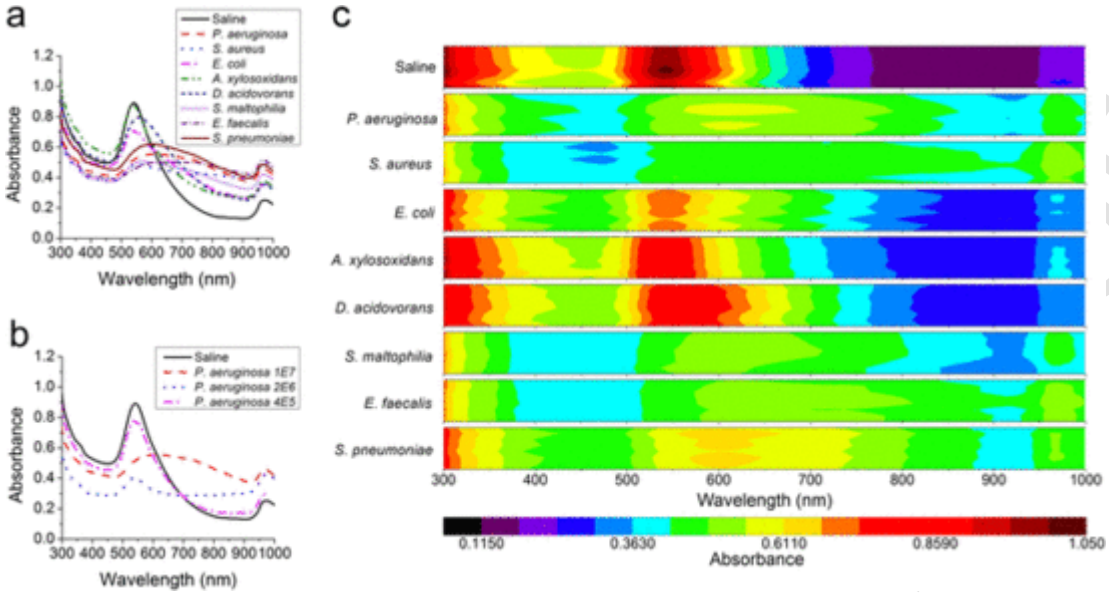

Fig. 6. Absorption spectra of gold nanoparticles in the presence of bacteria: (a) response for saline control and eight different species of bacteria normalized to $OD_{660} = 0.03$, (b) response in the presence of various concentrations (approximately 1×10^7, 2×10^6 and 4×10^5 CFU/well) of *Pseudomonas aeruginosa*, and (c) contour plot of replicates (n = 8) for each bacteria normalized to $OD_{660} = 0.03$ and saline control, where each band consists of 8 slices (one per replicate).

colorimetric responses are plotted in Fig. 6c and show minimal variation within species and drastic differences between species. This suggests that absorption spectra can be used for identification of the organism. Additionally, the colorimetric response highlighted by the absorption curves is also concentration dependent, as shown in Fig. 6b, where *P. aeruginosa* was normalized to a final $OD_{660} = 0.03$ and then diluted 5x and 25x in saline. Similarly, all other bacteria were also diluted and their spectra are presented as contour plots in Figs. S3 and S4. It can be observed that as the concentration of bacteria decreases, the differences between bacteria start to diminish yet subtle unique features remain. This data can now be used for training the "chemical nose" and determining the platform's ability to identify and quantify bacteria.

HCA is a useful technique for visualizing data with multiple dimensions (Lim et al., 2009). Three out of eight replicates will be used for training the "chemical nose" while the other five will be randomized for identification of unknown samples. We performed HCA on the three training replicates using each wavelength of the absorption spectra as a variable. The dendrogram resulting from HCA is presented in Fig. 7A for bacteria that were normalized to $OD_{660} = 0.03$. The dendrogram shows that there is no misclassification, since all the replicates have minimal Euclidean distance. In general, the dendrogram seems to separate Gram-positive and Gram-negative bacteria, where Gram-negative bacteria provide a lower response and are clustered closer to saline. Yet, *P. aeruginosa* and *S. maltophilia* provide a drastic enough response to be clustered together with the Gram-positive bacteria and as seen in TEM images and simulations, these pecu-

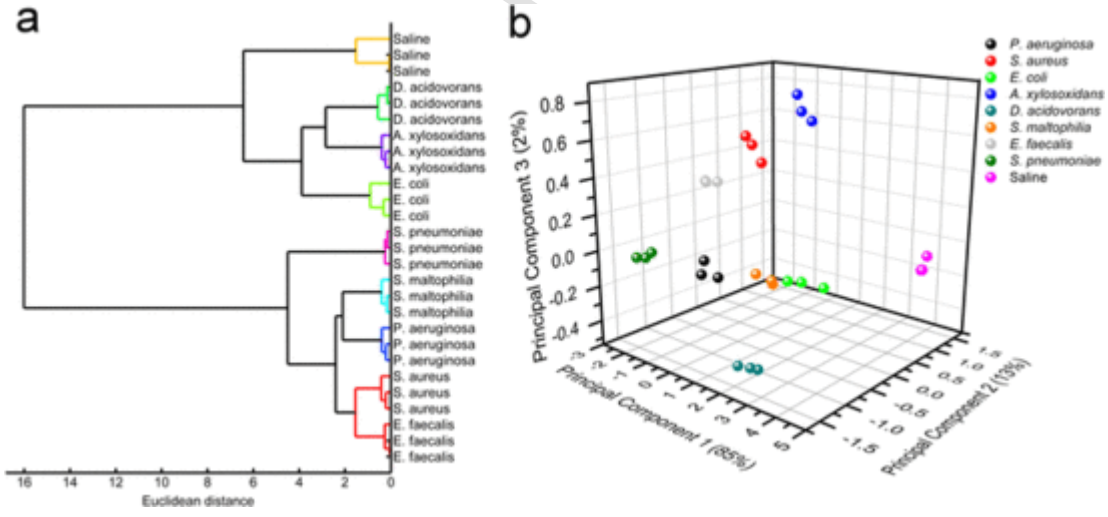

Fig. 7. (a) Dendrogram obtained using hierarchical clustering analysis (HCA) on the spectra (Ward's linkage method) of gold nanoparticles in the presence of bacteria normalized to $OD_{660} = 0.03$. The color threshold was set to 10% of the maximum Euclidean distance using MathWorks® MATLAB®. (b) Principal component analysis (PCA) scores plot of the gold nanoparticle response in the presence of bacteria. The percent variability explained is indicated on the axes. PCA model was built in MathWorks® MATLAB® using the spectral data in the range of 300–999 nm.

liarities are because of patterns of aggregation of nanoparticles. In order to use this data for identification of unknown samples, PCA is suitable for reduction of the dimensions. PCA on each of the eight bacteria at three different concentrations each demonstrated that the first three principal components could explain 100% of the variability amongst bacterial samples. PCA scores for bacteria normalized to $OD_{660} = 0.03$ are presented in Fig. 7b and they confirm the observations from HCA by highlighting clustering of the same bacterial species. The PCA scores for all other concentrations and the HCA dendrogram derived from these scores are presented in Fig. S5 and Fig. S6 respectively. The principal components were used to classify the other five replicates for each of the 25 groups (saline and three concentrations for each of the eight bacteria) using the coefficients from PCA model followed by LDA. An accuracy of 89% (111/125) was achieved, which is impressive because this suggests that an unknown sample can be characterized using the gold nanoparticle-based "chemical nose" platform to not only detect the presence of bacteria, but also identify the species and approximate concentration based on the colorimetric response. The accuracy from this study can be compared to a previous study where a similar system was used to detect four different species at a single concentration with an accuracy of 99% (Verma et al., 2014b). Most of the error in the current study results from misclassification of bacterial samples at the lowest concentrations, as indicated by the clusters in Fig. S6. All bacteria tested demonstrate a concentration dependent response as highlighted in Fig. S7. We hypothesize that the working concentration of the biosensor can be expanded using a more complex mixture of nanoparticles with various sizes, shapes, or functionalities, by assisting in discriminating bacteria at lower concentrations (Verma et al., 2015a). We have demonstrated that the concentration of nanoparticle also plays a significant role in determining the limit of detection (LOD) and an LOD of 5×10^4 CFU/mL was achieved using 10x diluted branched gold nanoparticles when detecting *P. aeruginosa* (Fig. S8) (Verma et al., 2015a). Although the current system cannot simultaneously identify and quantify bacteria at arbitrary concentrations with high accuracy (because of overlapping responses as seen in Fig. S7), if the identity of bacteria is known, it can be used for quantification and vice versa.

3.5. Detection of polymicrobial mixtures

Hospitals have become a major source of antibiotic-resistant infections and are a threat for vulnerable patients. Three of the most common hospital-isolated pathogens are: *S. aureus, E. coli,* and *P. aeruginosa* (Zhanel et al., 2013; Lockhart et al., 2007). These pathogens often exhibit unique antibiotic susceptibility profiles, which evolve over time and require timely monitoring using antibiograms (Joshi, 2010). In order to administer the appropriate antibiotic therapy, there is an urgent need for a biosensor to distinguish between bacterial species. Additionally, the detection of multiple bacterial species is especially important in the diagnosis of polymicrobial infections because certain species such as *P. aeruginosa* can express increased virulence in the presence of other bacteria (Korgaonkar et al., 2013). The "chemical nose" based on gold nanoparticles can be trained to detect mixtures of bacterial species. Binary and tertiary mixtures of *P. aeruginosa, S. aureus,* and *E. coli* were prepared (final OD_{660}=0.03, 1:1 v/v or 1:1:1 v/v/v) and then mixed with gold nanoparticles. The responses obtained from these mixtures are presented in Fig. 8a and appear to be dominated by the bacteria that cause higher aggregation. For example, in the case of a binary mixture of *P. aeruginosa* and *E. coli*, even though a pure *E. coli* sample does not cause a drastic color change, the mixture does cause a significant drop in the absorption peak and yet, the response is distinct from pure *E. coli* and *P. aeruginosa* cultures. Thus, in the case of infections, the "chemical nose" has the potential to distinguish between monomicrobial and polymicrobial instances, which will facilitate a more effective and rapid antimicrobial treatment without the need for extensive and lengthy testing of the sample. We analyzed this data using PCA and the scores are presented in Fig. 8b, where the variance was explained completely by using the first three components. Although the third principal component only accounts for 0.4% of the variance, this value is still significant compared to the variance between replicates, which is in the range of 0.01–0.04% for the saline and bacterial samples. Once again, three replicates were used for training the system and the other five were randomized for blind identification. An accuracy of 100% (40/40 samples) was obtained for each of the pure cultures and mixtures using LDA. Thus, the "chemical nose" can not only detect and discriminate between pure cultures but also identify species in mixed cultures. Given enough training sets, the "chemical nose" platform presented here can identify approximate concentrations of species in mixtures. Adding more nanoparticles with unique shapes such as gold nanorods, nanocubes, and nanoprisms can then expand the specificity and range of application for the "chemical nose" platform (Verma et al., 2015a). It should also be possible to detect and identify other pathogens such as

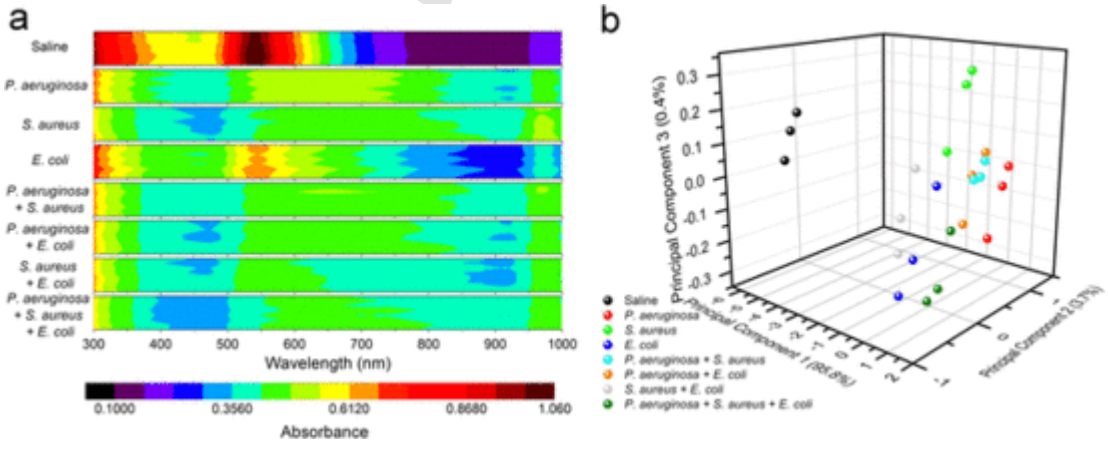

Fig. 8. Response of gold nanoparticles in the presence of mixtures of bacteria: (a) Contour plots of absorption spectra showing replicates for each sample (n = 8, one slice per replicate), (b) principal component analysis scores for three of the replicates that were used as training sets in linear discriminant analysis. The variance explained by each component is included in parenthesis with axes labels.

viruses, protozoa, and fungi by tuning the nanoparticle size and surface functionality.

4. Conclusion

We demonstrated that EPS play an important role in influencing the degree of nanoparticle aggregation around bacteria by shielding the effects of cell wall components. Additionally, simulations using the Maxwell-Garnett effective medium theory suggest that different aggregation patterns on bacterial cell walls are responsible for providing distinguishable colorimetric responses. We are able to use gold nanoparticles with varying morphologies as a versatile "chemical nose" platform for detecting, identifying, and quantifying species of pathogenic bacteria. The "chemical nose" can also distinguish between polymicrobial samples of the most prevalent pathogens in hospitals. The simplicity of detection in this system allows for field implementation without extensive technical expertise or training. This is especially important for developing countries, because of their limited resources and education. Thus, gold nanoparticles can be utilized for point-of-care diagnostics in the health industry and in-field testing in food and environmental industries by controlling their morphologies and training the "chemical nose" system.

Author contributions

The manuscript was written through contributions of all authors. All authors have given approval to the final version of the manuscript.

Notes

The authors declare no competing financial interests.

Acknowledgment

We would like to acknowledge Dr. Hsueh-Liang Chu and Professor Chia-Ching Chang from the National Chiao Tung University for their advice on lipid blot assays. This work was financially supported by the Natural Sciences and Engineering Research Council of Canada (NSERC) and 20/20 NSERC – Ophthalmic Materials Network. M.S.V. is grateful for the NSERC Vanier Canada Graduate Scholarship and the Banting Postdoctoral Fellowship. S.-C.W. is grateful to National Science Council of Taiwan for Project no. 103-2917-I-002-168. J.L.R. is thankful to the Waterloo Institute for Nanotechnology (WIN) Nanofellowship. P.Z.C. and J.M.T. are thankful for the NSERC Undergraduate Student Research Award.

Appendix A. Supplementary material

Supplementary data associated with this article can be found in the online version at doi:10.1016/j.bios.2016.04.024.

References

Abadeer, N.S., Fulop, G., Chen, S., Kall, M., Murphy, C.J., 2015. ACS Appl. Mater. Interfaces 7, 24915–24925.
Bajaj, A., Miranda, O.R., Kim, I.B., Phillips, R.L., Jerry, D.J., Bunz, U.H., Rotello, V.M., 2009. Proc. Natl. Acad. Sci. USA 106, 10912–10916.
Bajaj, A., Rana, S., Miranda, O.R., Yawe, J.C., Jerry, D.J., Bunz, U.H.F., Rotello, V.M., 2010. Chem. Sci. 1, 134–138.
Berry, V., Gole, A., Kundu, S., Murphy, C.J., Saraf, R.F., 2005. J. Am. Chem. Soc. 127, 17600–17601.
Berry, V., Saraf, R.F., 2005. Angew. Chem. Int. Ed. Engl. 44, 6668–6673.
Bohren, C.F., Huffman, D.R., 2008. Absorption and Scattering of Light by Small Particles. John Wiley & Sons.
Bunz, U.H., Rotello, V.M., 2010. Angew. Chem. Int. Ed. Engl. 49, 3268–3279.
Chung, H.J., Castro, C.M., Im, H., Lee, H., Weissleder, R., 2013. Nat. Nanotechnol. 8, 369–375.
Dantam, J., Zhu, H., Stapleton, F., 2011. Invest. Ophthalmol. Vis. Sci. 52, 51–57.
De, M., Rana, S., Akpinar, H., Miranda, O.R., Arvizo, R.R., Bunz, U.H., Rotello, V.M., 2009. Nat. Chem. 1, 461–465.
Donnelly, T., Doggett, B., Lunney, J., 2006. Appl. Surf. Sci. 252, 4445–4448.
Dowler, S., Kular, G., Alessi, D.R., 2002. Sci. STKE 2002 (pl6).
Dumont, E., Dugnoille, B., 1997. J. Non Cryst. Solids 218, 307–311.
El-Boubbou, K., Gruden, C., Huang, X., 2007. J. Am. Chem. Soc. 129, 13392–13393.
Epand, R.M., Epand, R.F., 2009. Biochim. Biophys. Acta 1788, 289–294.
Folmer-Andersen, J.F., Kitamura, M., Anslyn, E.V., 2006. J. Am. Chem. Soc. 128, 5652–5653.
Ghosh, S.K., Pal, T., 2007. Chem. Rev 107, 4797–4862.
Hayden, S.C., Zhao, G., Saha, K., Phillips, R.L., Li, X., Miranda, O.R., Rotello, V.M., El-Sayed, M.A., Schmidt-Krey, I., Bunz, U.H., 2012. J. Am. Chem. Soc. 134, 6920–6923.
Hong, Y., Brown, D.G., 2006. Colloids Surf. B Biointerfaces 50, 112–119.
Joshi, S., 2010. Indian J. Med. Microbiol. 28, 277–280.
Jung, J.H., Cheon, D.S., Liu, F., Lee, K.B., Seo, T.S., 2010. Angew. Chem. -Int. Ed. 49, 5708–5711.
Korgaonkar, A., Trivedi, U., Rumbaugh, K.P., Whiteley, M., 2013. Proc. Natl. Acad. Sci. USA 110, 1059–1064.
Lazcka, O., Del Campo, F.J., Munoz, F.X., 2007. Biosens. Bioelectron. 22, 1205–1217.
Li X. Kong H. Mout R. Saha K. Moyano D.F. Robinson S.M. Rana S. Zhang X. Riley M.A Rotello V.M. 2014. ACS Nano 8 12014–12019
Lim, S.H., Feng, L., Kemling, J.W., Musto, C.J., Suslick, K.S., 2009. Nat. Chem. 1, 562–567.
Liu, H., Fang, H.H., 2002. J. Biotechnol. 95, 249–256.
Liu, J., Lu, Y., 2006. Nat. Protoc. 1, 246–252.
Lockhart, S.R., Abramson, M.A., Beekmann, S.E., Gallagher, G., Riedel, S., Diekema, D.J., Quinn, J.P., Doern, G.V., 2007. J. Clin. Microbiol. 45, 3352–3359.
Lu, W., Singh, A.K., Khan, S.A., Senapati, D., Yu, H., Ray, P.C., 2010. J. Am. Chem. Soc. 132, 18103–18114.
Matsumoto, K., Kusaka, J., Nishibori, A., Hara, H., 2006. Mol. Microbiol. 61, 1110–1117.
Miranda, O.R., Creran, B., Rotello, V.M., 2010. Curr. Opin. Chem. Biol. 14, 728–736.
Moskovits, M., Hulse, J., 1977. J. Chem. Phys. 66, 3988–3994.
Niklasson, G.A., Granqvist, C.G., Hunderi, O., 1981. Appl. Opt. 20, 26–30.
Peng, G., Tisch, U., Adams, O., Hakim, M., Shehada, N., Broza, Y.Y., Billan, S., Abdah-Bortnyak, R., Kuten, A., Haick, H., 2009. Nat. Nanotechnol. 4, 669–673.
Phillips, R.L., Miranda, O.R., You, C.C., Rotello, V.M., Bunz, U.H., 2008. Angew. Chem. Int. Ed. Engl. 47, 2590–2594.
Rakic, A., Djurisic, A., Elazar, J., Majewski, M., 1998. Appl. Opt. 37, 5271–5283.
Rana, S., Le, N.D., Mout, R., Saha, K., Tonga, G.Y., Bain, R.E., Miranda, O.R., Rotello, C.M., Rotello, V.M., 2015. Nat. Nanotechnol. 10, 65–69.
Ricci, R.W., Ditzler, M., Nestor, L.P., 1994. J. Chem. Educ. 71, 983.
Rotello, V., 2009. Cell. Cycle 8, 3615–3616.
Sun, J., Ge, J., Liu, W., Wang, X., Fan, Z., Zhao, W., Zhang, H., Wang, P., Lee, S., 2012. Nano Res. 5, 486–493.
Swinehart, D.F., 1962. J. Chem. Educ. 39, 333.
Torres-Chavolla, E., Alocilja, E.C., 2009. Biosens. Bioelectron. 24, 3175–3182.
Ung, T., Liz-Marzan, L., Mulvaney, P., 2002. Colloid Surf. A-Physicochem. Eng. Asp. 202, 119–126.
Verma, M.S., Chen, P.Z., Jones, L., Gu, F.X., 2014. RSC Adv. 4, , 10660–10668.
Verma, M.S., Chen, P.Z., Jones, L., Gu, F.X., 2014. Biosens. Bioelectron. 61, , 386–390.
Verma M.S. Chen P.Z. Jones L. Gu F.X. 2015. Sens. Bio-Sens. Res.
Verma M.S. Rogowski J.L. Jones L. Gu F.X. 2015. Biotechnol. Adv.
Vierck, J.L., Bryne, K.M., Dodson, M.V., 2000. Methods Cell Sci. 22, 313–318.
Wan, Y., Sun, Y., Qi, P., Wang, P., Zhang, D., 2014. Biosens. Bioelectron. 55, 289–293.
Wang, D.S., Lin, C.W., 2007. Opt. Lett. 32, 2128–2130.
Wright, A.T., Zhong, Z., Anslyn, E.V., 2005. Angew. Chem. Int. Ed. Engl. 44, 5679–5682.
Yang, C., Xie, H., Li, Q.C., Sun, E.J., Su, B.L., 2015. J. Colloid Interface Sci. 450, 388–395.
Zambre, A., Chanda, N., Prayaga, S., Almudhafar, R., Afrasiabi, Z., Upendran, A., Kannan, R., 2012. Anal. Chem. 84, 9478–9484.
Zhanel, G.G., Adam, H.J., Baxter, M.R., Fuller, J., Nichol, K.A., Denisuik, A.J., Lagace-Wiens, P.R., Walkty, A., Karlowsky, J.A., Canadian Antimicrobial Resistance Alliance 2013. J. Antimicrob. Chemother. 68 (Suppl 1), i7–22.